Title: Impact of Equilibrative Nucleoside Transporters TgAT1, TgENT1, and TgENT3 on *Toxoplasma gondii* Infection and Differentiation.

Amber Goerner[1a], Gabriel Messina[1a], Lea Drogalis Beckham[1], Bruno Martorelli Di Genova[1*]
[1] – Department of Microbiology and Molecular Genetics, University of Vermont, Burlington, United States

[a] – co-first authors
[*] – corresponding author: bruno.mdigenova@med.uvm.edu

Abstract
The protozoan parasite *Toxoplasma gondii* relies on its host for essential metabolites, including purines, which it cannot synthesize de novo. This study investigates the roles of equilibrative nucleoside transporters (TgENTs), specifically TgAT1, TgENT1, and TgENT3, across different developmental stages of *T. gondii*. Utilizing protein-protein BLAST and position-specific iterated BLAST, we identified six genes in the *T. gondii* genome with high sequence similarity to human and *Plasmodium falciparum* ENTs, focusing on TgENT1, TgENT3, and TgAT1 due to their expression in tachyzoites and homology to the nucleoside domain.
Our results demonstrate that TgENT3 plays a crucial role during chronic infection, as TgENT3 deletion reduced tissue cysts by 50%. The double knockout of TgAT1 and TgENT3 (ΔTgAT1ΔTgENT3) failed to differentiate into bradyzoites under alkaline stress, indicating that both transporters are important for differentiation. Upregulation of TgENT1 transcripts in ΔTgAT1ΔTgENT3 parasites suggests a compensatory mechanism among TgENTs.
Conditional deletion of TgENT1 revealed its critical role in parasite growth and replication, with auxin-treated parasites showing reduced replication and long-term growth defects. Localization studies using immunofluorescence assays confirmed TgENT1's association with the plant-like vacuole (PLVAC) membrane, distinguishing it from other ENTs typically found at the plasma membrane.
These findings highlight the distinct and overlapping functions of TgENTs in *T. gondii*, emphasizing their potential as therapeutic targets for toxoplasmosis. Our study contributes to the broader understanding of nucleoside transporter functions in protozoans and suggests new avenues for drug development targeting ENT function to impair parasite survival and infection.

Introduction

De novo nucleic acid synthesis and salvage pathways are fundamental for cellular growth and survival, allowing cells to adapt to varying environmental conditions. Higher eukaryotes possess sophisticated mechanisms to modulate nucleoside transport, salvage, and metabolism, integrating intracellular and extracellular cues to maintain nucleotide homeostasis [1–5].

Many early branching eukaryotes, including the protozoan parasite *Toxoplasma gondii*, have evolved to survive and proliferate within host cells despite fluctuating concentrations of nucleosides and nucleobases. As an obligate intracellular parasite, *T. gondii* heavily depends on the host's metabolic machinery, scavenging essential metabolites, nutrients, and vitamins to support its growth [6–8]. One critical group of metabolites that *T. gondii* cannot synthesize *de novo* is purines, making the parasite rely entirely on host-derived purines for survival [6,7,9]. This reliance underscores the importance of understanding the mechanisms of purine acquisition in *T. gondii*. In host cells such as macrophages and neurons, purine levels are tightly regulated, presenting a challenging environment for the parasite [5,10].

The parasite employs equilibrative nucleoside transporters (TgENTs) as its primary means of scavenging purines from the host. *T. gondii* utilizes two purine salvage pathways: the phosphorylation of adenosine by the enzyme adenosine kinase and the phosphoribosylation of purine nucleobases by hypoxanthine-guanine phosphoribosyltransferase (HXGPRT) [9]. These pathways enable the parasite to salvage both adenosine and purine nucleobases efficiently. Additionally, *T. gondii* possesses a functional *de novo* pyrimidine biosynthesis pathway, with uracil phosphoribosyltransferase (UPRT) facilitating pyrimidine salvage by converting uracil to uridine monophosphate [9].

The initial identification of equilibrative nucleoside transporter (ENT) activity in *T. gondii* was demonstrated in extracellular tachyzoites, where adenosine, inosine, and hypoxanthine were transported into the parasite [11]. Subsequent studies identified TgAT1 via insertional mutagenesis[12]. Radioactive nucleoside incorporation assays revealed the presence of multiple nucleoside transporters in *T. gondii*, suggesting a complex system with at least one high-affinity adenosine transporter yet to be characterized [13]. TgAT1 activity remains the only TgENT studied *in vitro* using heterologous expression systems [14].

In this study, we aim to elucidate the roles of TgAT1 and other two homologs, TgENT1, and TgENT3, across different developmental stages of *T. gondii*. By comprehensively characterizing these transporters, we seek to enhance our understanding of their contributions to the parasite's survival and proliferation within the host, potentially identifying novel therapeutic targets for toxoplasmosis.

Results:

TgENT BLAST Analysis: We performed protein-protein BLAST or position-specific iterated BLAST on NCBI using Human ENT-1[15] and *Plasmodium falciparum* PfENT1[16] nucleoside transporters as query sequences to search for *T. gondii* sequences with high similarity. From the searches, 6 genes have been identified in the *T. gondii* genome with high sequence similarity to equilibrative nucleoside transporters (ENTs): TGME49_233130 (TgENT3), TGME49_244440 (TgAT1), TGME49_288540 (TgENT1),

TgME49_500147 (TgENT2), TgME49_320270, and TGME49_210820. From these six sequences, only four have homology to the ENT domain (**Fig. 1**). The data is summarized in **Table 1**.
Additionally, we compared TgAT1, TgENT1, and TgENT3 pore width to the human ENT crystal structure [17]. Our analyses revealed that the pore widths of all predicted TgENT structures are similar to that of human ENT1 (**Table 2**).
In this study, we focused on the TgAT1, TgENT1, and TgENT3, as they are expressed in tachyzoites in all available RNAseq data (ToxoDB) and have homology with the nucleoside domain (**Table 1** and **Fig. 1**).

Role of TgENT3 in chronic infection: According to previous transcriptomic data, TgENT3 is expressed during the chronic stages. We evaluated how TgENT3 deletion modulates parasite survival at the chronic stage in a mouse model. First, CBA/J mice were infected with the parental, ΔTgENT3, TgENT3-Ty (complemented), and after 28 days, tissue cysts were quantified by indirect immunofluorescence using *Dolichos biflorus* Agglutinin (DBA) as a cyst wall marker [18]. The number of tissue cysts in mice infected with ΔTgENT3 parasites was reduced by 50% compared with that in the Parental or TgENT3-Ty complement strains (**Fig. 2E).**
Mice infected with ΔTgENT3 had significantly improved survival and produced fewer tissue cysts, suggesting that TgENT3 is important during chronic infection (**Fig. 2D**). To evaluate if the decrease in cysts was associated with a defect in the acute infection stage, a group of mice was infected with each strain for only 10 days. Subsequently, their lungs were harvested, and a B1 quantitative PCR analysis was performed to quantify parasite burden in the tissue[19]. The results showed no significant differences in parasitemia between ΔTgENT3 and the parental and complemented lines at day 10 (**Fig. 2C**), further suggesting that the knockout strain phenotype is specific to the chronic stage.

Loss of TgAT1 and TgENT3 enhances chronic infection phenotype: TgAT1 is the only other TgENT homolog, besides TgENT3, predicted to localize to the plasma membrane (**Table 1**). Also, TgAT1 is the only TgENT homolog whose activity has been demonstrated *in vitro* [14]. Therefore, we investigated the effects of the simultaneous deletion of TgENT3 and TgAT1 on chronic infection. The growth rate was determined by growing the parasites in tachyzoite conditions for 48 and 72 hours before being fixed and stained with SAG1 through immunofluorescence assay (**Fig Supplemental 1**). The double knockout (ΔTgAT1ΔTgENT3) line did not exhibit a significant decrease in tachyzoite growth rate compared to the single TgENT knockout line (**Fig Supplemental 1**). However, given the phenotype of TgENT3 in chronic infection (**Fig. 2**), we induced parasite differentiation under alkaline stress conditions. The ΔTgAT1ΔTgENT3 parasites failed to differentiate into bradyzoites upon induction (**Fig. 3**), whereas the single knockout lines were DBA positive. Interestingly, approximately 60% of ΔTgAT1ΔTgENT3 parasite vacuoles were also negative for the acute stage marker SAG1, indicating that while these parasites respond to alkaline stress, they are still unable to differentiate into bradyzoites. (**Fig. 3**).
To test the hypothesis that ΔTgAT1ΔTgENT3 tachyzoites grow at a rate comparable to the single knockout lines due to compensation by another TgENT, we conducted quantitative PCR (qPCR) analysis. This analysis compared the expression levels of the remaining TgENTs, TgENT1 and TgENT2, in ΔTgAT1ΔTgENT3 tachyzoites, single

knockout lines, and the parental line. The qPCR results revealed an upregulation of TgENT1 transcripts in ΔTgAT1ΔTgENT3, while TgENT2 levels remain unchanged. In the following session, we will investigate the role of TgENT1 in tachyzoite growth (**Fig. 4**).

TgENT1 conditional deletion results in complete growth arrest: To investigate the role of TgENT1, characterized by a phenotype score of -3.6822[20] and resistance to gene deletion, we developed a parasite line (mAID-HA-TgENT1) with regulated TgENT1 expression via 3-indoleacetic acid (IAA) treatment[21]. We assessed the impact of TgENT1 depletion on parasite growth by culturing the parasites with IAA for 48 hours. The treated parasites exhibited reduced replication when invading fresh HS27 monolayers (**Fig. 4C**), indicating that TgENT1 expression is crucial for normal growth and replication. Additionally, a long-term growth defect was observed over nine days of continuous culture, as evidenced by the formation of smaller and fewer plaques (**Fig. 4D**).

TgENT1 localized to the PLVAC: Using the mAID-HA-TgENT1 construct, we were able to visualize the localization of TgENT1 within *T. gondii* parasites. When cultured with 500 µM indole-3-acetic acid (IAA), we observed the disappearance of the TgENT1 signal, confirming the system functionality (**Fig. 5**). Interestingly, the signal was not detected at the plasma membrane of the parasites. Instead, TgENT1 appeared as punctate structures within the cells (**Fig. 5**).

To determine the specific intracellular compartment associated with TgENT1, we employed immunofluorescence assays (IFA) using co-stains of various *Toxoplasma gondii* organelle markers. We selected *T. gondii* cathepsin protease L (TgCPL) and *T. gondii* chloroquine resistance transporter (TgCRT), both known to localize to the Plant-like Vacuole (PLVAC)[22].

Upon performing the IFA, we observed co-localization of HA-tagged TgENT1 with TgCRT, and a close co-localization with TgCPL. TgCRT, being a membrane-bound protein of the PLVAC, and TgCPL, which is stained in the lumen of the PLVAC, indicated that TgENT1 is embedded in the membrane of the PLVAC. This was visually confirmed through the co-localization patterns (**Fig. 5**). These findings suggest that TgENT1 is specifically associated with the PLVAC membrane within *T. gondii*, providing insights into its potential functional roles and subcellular targeting.

Discussion

The study identified six genes in *T. gondii* with sequence similarity to equilibrative nucleoside transporters (**Fig. 1**). These findings are significant given the critical roles that ENTs play in protozoan biology, particularly in nucleoside transport, which is essential for nucleotide synthesis and overall cellular metabolism.

ENTs mediate the facilitative transport of nucleosides and some nucleobases, playing crucial roles in maintaining nucleoside homeostasis within the cell [17,24]. Our study focused on TgENT1, TgENT3, and TgAT1, elucidating their roles in chronic and acute infection stages. The deletion of TgENT3 significantly reduced the number of tissue cysts and improved the survival of infected mice, indicating that TgENT3 is crucial for cyst formation and survival during the chronic stage (**Fig. 2**). These differences were less pronounced during invasion into tissue culture, suggesting a complex interaction with the host.

The TgENT3 and TgAT1 double knockout (ΔTgAT1ΔTgENT3) lines did not show a significant decrease in tachyzoite growth rate compared to the single TgENT3 knockout line in tissue culture (**Supplemental Fig. 1**). However, it failed to differentiate into bradyzoites under alkaline stress conditions, suggesting that both TgAT1 and TgENT3 activities are critical for the differentiation process (**Fig. 3**). The observed upregulation of TgENT1 transcripts in ΔTgAT1ΔTgENT3 parasites indicates a compensatory mechanism, highlighting the interconnected roles of different ENTs in maintaining nucleoside levels crucial for parasite survival and differentiation (**Fig. 4**).

The conditional deletion of TgENT1 demonstrated its crucial role in parasite growth and replication, as evidenced by the growth defects observed upon TgENT1 depletion (**Fig. 4**). This finding underscores the transporter's importance in maintaining adequate nucleoside levels for nucleotide biosynthesis, which is vital for rapid parasite replication and survival.

Localization studies revealed that TgENT1 is associated with the PLVAC membrane, differentiating it from other ENTs typically found at the plasma membrane (**Fig. 5**). This unique localization suggests specialized functions of TgENT1 within intracellular compartments, possibly related to specific metabolic processes or stress responses crucial for the parasite survival and differentiation. In humans, ENT3 is predominantly located in lysosomes and mitochondria, playing a significant role in intracellular nucleoside transport and lysosomal function [25]. The similarity in localization suggests a conserved function across species, where TgENT1 may facilitate nucleoside transport within the PLVAC akin to ENT3 in human lysosomes. This comparison highlights the evolutionary conservation of ENT functions and emphasizes the potential metabolic importance of TgENT1 within *T. gondii* 's unique organelles.

Our findings significantly contribute to the broader understanding of nucleoside transporter functions in protozoans, particularly concerning their roles in infection stages and intracellular compartmentalization. Our results suggest that these transporters have distinct roles (**Fig. 2** and **Fig. 4**). However, optimal parasite growth and differentiation is achieved through synergistic activity (**Fig. 3**). The overlap between transporters' roles and their potential redundancy is highlighted by the transcriptional changes (**Fig. 4A**) observed in the ΔTgAT1ΔTgENT3 strain. TgENT1 is only overexpressed in the ΔTgAT1ΔTgENT3 strain, not in the single transporter mutants. This phenotype indicates a possible compensatory mechanism and functional redundancy among the TgENTs that should be further studied. Studies of the human homologs ENT1 and ENT2 have shown divergent sequence identity; however, their roles overlap in the transport of nucleosides and nucleobases. This divergence may enable distinct physiological roles, yet it also permits redundancy in this critical mechanism within the organism [26]. Our work suggests that TgAT1 and TgENT3 exhibit some level of redundancy, as the loss of both is required to induce transcriptional changes in alternative transporters. Future research should focus on exploring the nucleoside transport activities of TgENT1 and TgENT3 and the regulatory mechanisms governing TgENT expression. The interactive and overlapping functions of these transporters raise questions not only about the roles of individual genes but also about the overall mechanism of nucleoside transport and the cooperative functioning of transporters in tandem.

The findings raise the question of the potential for targeting TgENT transporters as therapeutic strategies, suggesting a direction for future investigations. The results of this

study open new avenues for exploring *T. gondii* metabolic dependencies[8] and developing drugs that target ENT function, thereby impairing the parasite's ability to maintain infection. Further research could also investigate compensatory mechanisms involving other nucleoside transporters, potentially revealing additional targets for therapeutic intervention.

In conclusion, our research underscores the critical roles of TgAT1, TgENT1, and TgENT3 in *T. gondii's* lifecycle, highlighting their potential as targets for therapeutic development. These insights pave the way for future investigations into the metabolic pathways of *Toxoplasma gondii* and their exploitation for disease control.

Table 1 – BLAST results for *T. gondii* sequences with high similarity with Human ENT1 and *Plasmodium falciparum* ENT1.

Gene ID	Name	Localization by hyperLOPIT[27]	PFam ID	PFam Description	Phenotype Score[20]	Stage expression (ToxoDB)
TGME49_210820	210820	Rhoptry 2	N/A	N/A	-2.74	Tachyzoite, bradyzoite
TGME49_233130	TgENT3	PM integral, Golgi	PF01733	Equilibrative nucleoside transporter	0.04	Tachyzoite, bradyzoite, sex
TGME49_244440	TgAT1	PM integral, Golgi	PF01733	Equilibrative nucleoside transporter	1.02	Tachyzoite, bradyzoite, sex
TGME49_288540	TgENT1	None	PF01733	Equilibrative nucleoside transporter	-3.68	Tachyzoite, bradyzoite, sex
TGME49_320270	320270	None	N/A	N/A	-0.61	Bradyzoite, sex
TGME49_500147	TgENT2	None	PF01733	Equilibrative nucleoside transporter	0.47	Bradyzoite, sex

Figure 1 – Phylogenetic tree of the 6 *Toxoplasma* genes with high sequence similarity to human ENT1 (hENT1). (A) All six *T. gondii* genes sequences were aligned using MUSCLE[28]. Utilizing the alignment, we generated a phylogenetic tree by the Neighbor-Joining algorithm[29], with bootstrap values indicated at each node. The scale bar represents the evolutionary distance of 0.20 substitutions per site. The tree shows two distinct clades: the first includes TgAT1, TgENT2, TgENT1, and TgENT3, suggesting a closer evolutionary relationship among these proteins. The second clade includes TGME49_210820 and TGME49_320270, indicating a different evolutionary lineage. Bootstrap values support the reliability of these groupings, with values above 50% shown at the respective nodes. The human concentrative transporter 1 (hCNT1) was included as the outgroup. **(B)** Predicted three-dimensional structures of TgAT1, TgENT1, and

TgENT3. The models were generated using AlphaFold. The alpha-helical transmembrane domains are depicted in purple, illustrating the characteristic secondary structure of these transporters. The left panel shows the TgAT1 model, the center panel shows TgENT1, and the right panel shows TgENT3. Each structure highlights the conserved transmembrane helices typical. **(C)** Crystal structure of human ENT1 (PDBID: 6OB7) in cyan aligned with AlphaFold predicted models of TgENT1, TgENT3, and TgAT1 in purple.

Table 2 – Pore width and Root Mean Square Deviation (RMSD) comparing human ENT1(PDBID: 6OB7) to TgENT1, TgENT3, and TgAT1.

Structure	Pore width (long)(Å)	Pore width (short)(Å)	RMSD (relative to 6OB7) (Å)
hENT1	30.0	18.3	0
TgENT1	31.1	18.0	3.32
TgENT3	30.0	18.5	6.54
TgAT1	28.5	18.8	4.41

Figure 2 – Loss of TgENT3 results in chronic infection defect. (A) Growth assay of tachyzoite conditions, completed in normal media conditions and fixed following 48 or 72 hours of invasion and stained using immunofluorescence assay against SAG1 and DAPI. Calculations were made by randomly counting 100 vacuoles per coverslip per condition. Left image 48 hours, and the right image 72 hours. Significance determined using ANOVA analysis. **(B)** Differentiation from tachyzoite to bradyzoite assay was completed in alkaline stress media, fixed following 48 or 72 hours of invasion, and stained using **IFA** against SAG1, DBA and DAPI. Calculations were made by random counting of 100 vacuoles per coverslip per conditions. Left image 48 hours, right image 72 hours. Significance determined using ANOVA analysis. **(C)** Acute stage infection evaluation using mice infected for 10 days with 100 parasites per mouse. Following 10 days lungs were removed and evaluated using B1 gene analysis. Significance determined using ANOVA analysis. D. Survival curve of mice infected up to 30 days with 100 parasites per mouse. E. Chronic stage infection evaluation using mice infected for 30 days with 100 parasites per mouse. Brain was removed and evaluated by visual count of 1/100th of brain homogenate. Significance determined using ANOVA analysis.

Figure 3 – Simultaneous deletion of TgENT3 and TgAT1 enhances chronic defect. (A) Immunofluorescent staining illustrating alkaline stress-induced differentiation, nuclei were stained with DAPI (Cyan), tachyzoites were marked with anti-SAG1 (Yellow), and bradyzoites were identified using DBA lectin (Magenta). Differentiation was quantified by determining the percentage of differentiated vacuoles, based on counts of 100 randomly chosen vacuoles per coverslip at 2 (**B**) and 3 (**C**) days post invasion. Statistical significance was assessed using ANOVA.

Figure 4 –TgENT1 has a compensatory role and is essential for normal growth and replication.
(**A**) Quantitative PCR of TgENT1 and TgENT2 transcripts in our single and double KO strains. (**B**) Parasite growth as measured by number of parasites per vacuole and average vacuole size. Parasites were cultured for 48hrs intracellularly with or without 500uM IAA prior to start of assay. At least 50 vacuoles were counted for each replicate, 3 replicates for each condition. (**C**) Plaque assay; wells invaded with 50 parasites per well, with either +/- 500uM IAA, and stained with Crytal Violet after 9 days.

Figure 5 - Immunofluorescence Imaging Analysis of mAID-HA-TgENT1. We conducted immunofluorescence imaging on the mAID-HA-TgENT1 strain cultured with or without 500 μM IAA for 48 hours. Following this treatment period, the strains were allowed to invade HFF monolayers and were subsequently fixed after 36 hours. The prepared slides were stained for HA and various *Toxoplasma gondii* markers: **(A)** chloroquine resistance transporter (TgCRT), **(B)** cathepsin protease L (TgCPL), both known to associate with the PLVAC.

Methods

Cell Culture
Parasites were maintained in human foreskin fibroblast (HFF) cells using DMEM supplemented with 10% fetal bovine serum (FBS), penicillin and streptomycin.

AlphaFold Modeling
Predicted protein structures were retrieved from the AlphaFold Protein Structure Database (AlphaFold DB)[30] using their UniProt accession code. These predicted structures were aligned with human ENT1 (PDBID: 6OB7) using Pymol (Schrodinger). Atomic measurements of pore width also performed in Pymol. Measurement of human ENT1 pore in cyan. The width of the pore measured across the widest and narrowest points (yellow dashed line – **Fig 1C**) using Pymol. TgENT1, TgENT3, and TgAT1 pores were measured in the same manner.

Plasmids
All final plasmid sequences are listed in the plasmid list (supplemental file). Plasmids were constructed using standard molecular biology techniques according manufacturer's protocols.

- **ΔTgENT3 Donor:** Synthesized and ordered from Genscript.
- **TgENT3-TY1 Donor:** Constructed using plasmid ΔTgENT3 donor. Long PCR with Q5 polymerase using primers P1 and P2 amplified the backbone region and homology arms upstream and downstream of the TgENT3 gene region. Taq polymerase PCR with primers P3 and P4 amplified the TgENT3 gene minus the stop codon and added the TY1 epitope to t3' 3' end. Another PCR using Taq polymerase and primers P5 and P6 added homology to the backbone fragment. These fragments were assembled using Gibson Assembly (NEB).
- **ΔTgAT Donor:** Generated by digesting the ΔTgENT3 donor with AvrII and NotI to isolate the insert fragment and SpeI and AflII to isolate the backbone fragment. Fragments were purified using a gel agarose purification kit (NEB Monarch). Taq polymerase PCR with primers P7 and P8, or P9 and P10, amplify 5' and 3' homology to the TgAT gene, respectively. Fragments were purified and assembled using Gibson Assembly (NEB).
- **TgENT3-DHFR-KO Donor:** pUC6-DHFR was purchased from Addgene (plasmid #80329). Primers P11 and P12 amplified the DHFR region. The ΔTgENT3 donor was digested with NotI and EcoRV, and fragments were joined via Gibson Assembly (NEB).
- **mAID-HA-TgENT1 Donor:** Synthesized and ordered from Genscript (plasmid mAID-HA-TgENT1 donor).
- **Guide RNA Plasmids:** Pss013 CrispR guide vector was purchased from Addgene and digested with BsaI, then purified. gRNA oligos from IDT were cloned into Pss013 using Gibson Assembly (NEB). Plasmids were transformed into DH5α E. coli, sequenced, and expanded via Maxi prep (GeneJet).

DNA Preparation for Transfection
50 µg of donor plasmid per transfection was digested with enzymes as specified. Reactions proceeded over several days at 37°C. Complete digestion was confirmed via agarose gel electrophoresis. DNA was isolated using phenol/chloroform extraction, and 25 µg of each guide RNA plasmid per reaction was added. DNA was resuspended in 10 µL water following ethanol precipitation.

Mutant Strain Creation

Mutant *Toxoplasma gondii* strains were generated using CRISPR-Cas9 gene editing with a donor repair template plasmid and two gRNAs. Initial and mutant strains, along with plasmids, are listed in the supplemental file.

Transfection

Parasites were isolated from a fully confluent T25 flask, washed once with cytomix buffer (120 mM KCl, 0.15 mM CaCl2, 10 mM K2HPO4/KH2PO4 pH 7.6, 25 mM HEPES, 2 mM EGTA pH 7.6, MgCl2, final pH 7.6) and resuspended in 400 µL cytomix. 50 µg of donor and 25 µg of each guide were mixed with the parasites and placed in a 4 mm gap cuvette. Parasites were electroporated using BTX Electroporator settings and immediately invaded a fresh T25 flask of HS27 cells. Media was changed the next day, and selection drugs were added (pyrimethamine after 24 hours, chloramphenicol immediately).

- **ΔTgENT3 Strain:** 50 µg of ΔENT3 donor plasmid digested with AflII, combined with 25 µg each of guide plasmid gRNAs G1, G2, G3, and G4, ethanol precipitated, and resuspended in 10 µL water. Transfection of parental strain Me49 dKu80 followed the protocol above. Parasites were selected with 40 µM chloramphenicol for 2 weeks, then flow-sorted based on green fluorescence into a 96-well plate, 3 parasites per well. Clonal parasites were expanded and genotyped using primers P13 and P14 to confirm insert presence, and P15 and P16 to confirm WT sequence ablation.
- **ΔTgENT3::TgENT3-TY1:** 50 µg of TgENT3-TY1 donor plasmid digested with AflII, purified, and combined with 25 µg each of guide plasmid gRNAs G5, G6, G7, ethanol precipitated. Transfection of ΔTgENT3 strain followed the above protocol. After a week, parasites were flow sorted based on the lack of green fluorescence. Clonal parasites were expanded, genomes extracted, and genotyped using primers P15 and P16 to confirm the reinsertion of TgENT3 at the desired locus and P13 and P14 to confirm removal of the insert sequence.
- **ΔTgAT:** 50 µg of ΔTgAT donor plasmid digested with NheI, purified, combined with 25 µg each of guide plasmid gRNAs G8 and G9, ethanol precipitated. Transfection of parental strain Me49 dKu80 followed the protocol above. Parasites were selected with 40 µM chloramphenicol for 2 weeks, then flow-sorted based on green fluorescence into a 96-well plate, 3 parasites per well. Clonal parasites were expanded, genomes extracted, and genotyped using primers P17 and P18 to confirm the presence of the insert, and P19 and P20 to confirm WT genome ablation.
- **ΔTgATΔTgENT3:** 50 µg of TgENT3-DHFR-KO donor plasmid digested with ApaI, purified, combined with 25 µg each of guide plasmid gRNAs G1 and G2, ethanol precipitated. Transfection of Me49 dKu80 ΔTgAT strain followed the protocol above. Parasites were selected with 3 µM pyrimethamine for 2 weeks, manually cloned into 96-well plates (3 parasites per well), expanded, and genomes extracted. PCR with primers P21 and P22 confirmed insertion, while primers P15 and P16 confirmed disruption of TgENT3 locus.
- **mAID-HA-TgENT1:** 50 µg of mAID-HA-TgENT1 donor plasmid digested with AsiSI, purified, combined with 25 µg each of guide plasmid gRNAs G10 and G11, ethanol precipitated. Transfection of RH Tir1 strain followed the protocol above. Parasites were selected with 3 µM pyrimethamine for 2 weeks, manually cloned into 96-well plates (3 parasites per well), expanded, and genomes extracted. Genotyping with primers P23 and P24 confirmed insertion and was further confirmed by visualization of HA tag in an immunofluorescence assay.

Immunofluorescent Assay

- **Adherent Cells.** Cells were fixed in 3.7% formaldehyde for 20 minutes, washed twice with 1x PBS, blocked and permeabilized with 3% BSA and 0.2% Triton X-100 for at least 2 hours at room temperature (or up to one week at 4°C). Primary antibodies were diluted 1:500 in blocking/permeabilization solution and incubated for 1 hour at room temperature (or overnight at 4°C). Cells were washed twice with 1x PBS, secondary antibodies were applied at 1:500 dilution in blocking/permeabilization solution for 45-60 minutes at room temperature, washed three times for 5 minutes, and glass coverslips were mounted and sealed.
- **Homogenized Tissue.** The tissue was homogenized using serial needles passing through 18-, 20-, and 22-gauge needles, pelleted at 1000xg for 5 minutes, and fixed with 3.7% formaldehyde for 20 minutes. Pellets were washed twice with 1x PBS, blocked overnight in 1% BSA and 0.2% Triton X-100 in 1x PBS, primary antibodies diluted 1:500 were incubated overnight, washed twice with 1x PBS, secondary antibodies (1:500 dilution) and DAPI were added for 1 hour, washed twice with 1x PBS, and imaged using a microscope.

Differentiation HFF Assay

Confluent HFF cells were invaded with parasites for 4 hours. Stress conditions involved exchanging media for pH 8.2 media and incubating without CO2 to maintain pH. Media was refreshed daily. Control cells were maintained at pH 7.4. Cells were fixed at 48 and/or 72 hours and stained by immunofluorescence assay. Differentiation rate was determined by counting 100 vacuoles and identifying them as SAG1 positive, DBA positive, both positive, or neither.

Vacuole Counts

Stained slides of pH 7.4 invaded HFFs with each parasite strain were analyzed using a BIOTEK instrument. The number of parasites per vacuole was determined by counting 100 randomly chosen vacuoles.

Mouse Infection

Five CBA/j mice per strain were infected with 100 tachyzoite parasites diluted in 1x PBS via intraperitoneal injection and allowed to invade for 24 to 30 days. Mouse cortexes were harvested following CO2 and cervical dislocation euthanasia.

Raw Counts

Half of the cortexes were collected in 1.5 mL of 1x PBS and stored at 4°C overnight. Samples were homogenized by serial needle passing through 18-, 20-, and 22-gauge needles. A 1:100 dilution (30 µL) of the total cortex sample was placed on a slide, scanned at 4x objective for cysts, and recorded.

Immunofluorescence assays (IFA) of Cyst Sizes and Field Count

The homogenate from raw cyst data was spun down, fixed in 3.7% formaldehyde, permeabilized/blocked, and stained for DBA and DAPI.

- **Images:** 100x images were taken from wet mounts using an oil lens microscope.
- **Cyst Sizes:** Stained cysts were wet mounted onto coverslips and scanned for DBA using a BIOTEK microscope. 50 randomly found cysts per sample were measured and recorded using the BIOTEK software.
- **Field Counts:** Equal volumes of each sample were wet mounted into 24-well plates with coverslips, allowing the solution to spread evenly. 20 randomly chosen fields were counted for the number of cysts per field (totaling 40 fields per sample).

Parasite Burden

B1 gene analysis of mouse organs was completed following DNA extraction using the Qiagen kit, eluting in 50 µL of water. Samples were normalized based on DNA spectroscopy, using 600 ng of total DNA per reaction. Details of primer amounts, master mix, qPCR cycle, and machine/software specifications are provided (Primer set Q1 & Q2).[19]

Image Preparation

Images were collected at 20x using a Biotek cytation 7 microscope or at Leica DM ire2 100x using an oil lens microscope. Images were colored, and scale bars were added using ImageJ. Figures were created using Adobe Illustrator.

qPCR

RNA was extracted from freshly lysed tachyzoites using the GeneJet RNA Purification Kit. Complementary DNA (cDNA) was subsequently synthesized employing the Maxima H Minus First Strand cDNA Synthesis Kit. Quantitative PCR (qPCR) reactions were then set up with primers Q1 – Q8 using the PowerSYBR Green PCR Master Mix.

Acknowledgments

This research was supported by a research grant from National Institutes of Health (P20 GM125498). We thank Dr. Harry de Koning and Dr. Vern Carruthers for helpful discussions.

References

1. Verrier F, An S, Ferrie AM, Sun H, Kyoung M, Deng H, Fang Y, Benkovic SJ. GPCRs regulate the assembly of a multienzyme complex for purine biosynthesis. Nat Chem Biol. 2011 Oct 23;7(12):909–915. PMID: 22020552

2. Huang Z, Xie N, Illes P, Di Virgilio F, Ulrich H, Semyanov A, Verkhratsky A, Sperlagh B, Yu SG, Huang C, Tang Y. From purines to purinergic signalling: molecular functions and human diseases. Signal Transduct Target Ther. 2021 Apr 28;6(1):162. PMID: 33907179

3. Mason S. Signaling for purines. Nature Structural & Molecular Biology. 2011 Dec 1;18(12):1322–1322.

4. Jain S, Jacobson KA. Purinergic signaling in diabetes and metabolism. Biochem Pharmacol. 2021 May;187:114393. PMID: 33359363

5. Soler C, García-Manteiga J, Valdés R, Xaus J, Comalada M, Casado FJ, Pastor-Anglada M, Celada A, Felipe A. Macrophages require different nucleoside transport systems for proliferation and activation.

6. Kloehn J, Hammoudi PM, Soldati-Favre D. Metabolite salvage and restriction during infection — a tug of war between Toxoplasma gondii and its host. Current Opinion in Biotechnology. 2021 Apr 1;68:104–114. PMID: 33202353

7. Krishnan A, Kloehn J, Lunghi M, Chiappino-Pepe A, Waldman BS, Nicolas D, Varesio E, Hehl A, Lourido S, Hatzimanikatis V, Soldati-Favre D. Functional and Computational Genomics Reveal Unprecedented Flexibility in Stage-Specific Toxoplasma Metabolism. Cell Host Microbe. United States; 2020 Feb 12;27(2):290-306.e11. PMID: 31991093

8. Martin Blume, Martin Blume, Blume M, Seeber F. Metabolic interactions between Toxoplasma gondii and its host. F1000Research. 2018 Oct 30;7:1719.

9. Fox BA, Bzik DJ. Biochemistry and metabolism of Toxoplasma gondii: purine and pyrimidine acquisition in Toxoplasma gondii and other Apicomplexa. 2020 Jan 1;397–449.

10. Dunwiddie TV, Masino SA. The Role and Regulation of Adenosine in the Central Nervous System. Annu Rev Neurosci. 2001 Mar 1;24(1):31–55. PMID: 11283304

11. Conrad Schwab J, Afifi Afifi M, Pizzorno G, Handschumacher RE, Joiner KA. Toxoplasma gondii tachyzoites possess an unusual plasma membrane adenosine transporter. Molecular and Biochemical Parasitology. 1995 Mar 1;70(1):59–69. PMID: 7637715

12. Chiang CW, Carter N, Sullivan WJ, Donald RGK, Roos DS, Naguib FNM, Kouni MH el, Ullman B, Wilson CM. The Adenosine Transporter of Toxoplasma gondii: IDENTIFICATION BY INSERTIONAL MUTAGENESIS, CLONING, AND

RECOMBINANT EXPRESSION *. Journal of Biological Chemistry. Elsevier; 1999 Dec 3;274(49):35255–35261. PMID: 10575012

13. De Koning HP, Al-Salabi MI, Cohen AM, Coombs GH, Wastling JM. Identification and characterisation of high affinity nucleoside and nucleobase transporters in Toxoplasma gondii. International Journal for Parasitology. 2003 Jul 30;33(8):821–831.

14. Campagnaro GD, Elati HAA, Balaska S, Martin Abril ME, Natto MJ, Hulpia F, Lee K, Sheiner L, Van Calenbergh S, de Koning HP. A Toxoplasma gondii Oxopurine Transporter Binds Nucleobases and Nucleosides Using Different Binding Modes. International Journal of Molecular Sciences. 2022 Jan;23(2):710. PMID: 35054895

15. Wright NJ, Lee SY. Structures of human ENT1 in complex with adenosine reuptake inhibitors. Nature Structural & Molecular Biology. 2019 Jul 1;26(7):599–606.

16. Wang C, Yu L, Zhang J, Zhou Y, Sun B, Xiao Q, Zhang M, Liu H, Li J, Li J, Luo Y, Xu J, Lian Z, Lin J, Wang X, Zhang P, Guo L, Ren R, Deng D. Structural basis of the substrate recognition and inhibition mechanism of Plasmodium falciparum nucleoside transporter PfENT1. Nat Commun. England; 2023 Mar 28;14(1):1727. PMCID: PMC10050424

17. Wright NJ, Lee SY. Structures of human ENT1 in complex with adenosine reuptake inhibitors. Nat Struct Mol Biol. United States; 2019 Jul;26(7):599–606. PMCID: PMC6705415

18. Waldman BS, Schwarz D, Wadsworth MH, Saeij JP, Shalek AK, Lourido S. Identification of a Master Regulator of Differentiation in Toxoplasma. Cell. 2020 Jan 23;180(2):359-372.e16.

19. Lin MH, Chen TC, Kuo T tong, Tseng CC, Tseng CP. Real-Time PCR for Quantitative Detection ofToxoplasma gondii. Journal of Clinical Microbiology. American Society for Microbiology; 2000 Nov;38(11):4121–4125.

20. Sidik SM, Huet D, Ganesan SM, Huynh MH, Wang T, Nasamu AS, Thiru P, Saeij JPJ, Carruthers VB, Niles JC, Lourido S. A Genome-wide CRISPR Screen in Toxoplasma Identifies Essential Apicomplexan Genes. Cell. 2016 Sep 8;166(6):1423-1435.e12. PMID: 27594426

21. Brown KM, Long S, Sibley LD. Conditional Knockdown of Proteins Using Auxin-inducible Degron (AID) Fusions in Toxoplasma gondii. Bio Protoc. 2018 Feb 20;8(4):e2728. PMCID: PMC5890294

22. Stasic AJ, Moreno SNJ, Carruthers VB, Dou Z. The Toxoplasma plant-like vacuolar compartment (PLVAC). J Eukaryot Microbiol. United States; 2022 Nov;69(6):e12951. PMCID: PMC10576567

23. McGovern OL, Rivera-Cuevas Y, Kannan G, Narwold AJJ, Carruthers VB. Intersection of endocytic and exocytic systems in Toxoplasma gondii. Traffic. England; 2018 May;19(5):336–353. PMCID: PMC6787929

24. Boswell-Casteel RC, Hays FA. Equilibrative nucleoside transporters-A review. Nucleosides Nucleotides Nucleic Acids. 2017 Jan 2;36(1):7–30. PMCID: PMC5728162

25. Hsu CL, Lin W, Seshasayee D, Chen YH, Ding X, Lin Z, Suto E, Huang Z, Lee WP, Park H, Xu M, Sun M, Rangell L, Lutman JL, Ulufatu S, Stefanich E, Chalouni C, Sagolla M, Diehl L, Fielder P, Dean B, Balazs M, Martin F. Equilibrative nucleoside transporter 3 deficiency perturbs lysosome function and macrophage homeostasis. Science. United States; 2012 Jan 6;335(6064):89–92. PMID: 22174130

26. Hau RK, Wright SH, Cherrington NJ. Addressing the Clinical Importance of Equilibrative Nucleoside Transporters in Drug Discovery and Development. Clin Pharmacol Ther. United States; 2023 Oct;114(4):780–794. PMID: 37404197

27. Barylyuk K, Koreny L, Ke H, Butterworth S, Crook OM, Lassadi I, Gupta V, Tromer E, Mourier T, Stevens TJ, Breckels LM, Pain A, Lilley KS, Waller RF. A Comprehensive Subcellular Atlas of the Toxoplasma Proteome via hyperLOPIT Provides Spatial Context for Protein Functions. Cell Host & Microbe. 2020 Nov 11;28(5):752-766.e9.

28. Edgar RC. MUSCLE: multiple sequence alignment with high accuracy and high throughput. Nucleic Acids Res. England; 2004;32(5):1792–1797. PMCID: PMC390337

29. Tamura K, Nei M, Kumar S. Prospects for inferring very large phylogenies by using the neighbor-joining method. Proc Natl Acad Sci U S A. United States; 2004 Jul 27;101(30):11030–11035. PMCID: PMC491989

30. Jumper J, Evans R, Pritzel A, Green T, Figurnov M, Ronneberger O, Tunyasuvunakool K, Bates R, Žídek A, Potapenko A, Bridgland A, Meyer C, Kohl SAA, Ballard AJ, Cowie A, Romera-Paredes B, Nikolov S, Jain R, Adler J, Back T, Petersen S, Reiman D, Clancy E, Zielinski M, Steinegger M, Pacholska M, Berghammer T, Bodenstein S, Silver D, Vinyals O, Senior AW, Kavukcuoglu K, Kohli P, Hassabis D. Highly accurate protein structure prediction with AlphaFold. Nature. Nature Publishing Group; 2021 Aug;596(7873):583–589.

Supplemental material:

Supplemental Figure 1: (A) Immunofluorescence assay of the growth curve in normal pH conditions. Nuclei staining using DAPI (Cyan), Tachyzoite marker using anti-SAG1 (Yellow), bradyzoite marker using DBA lectin (Magenta). **(B)** Quantification of growth curve by randomly counting 100 vacuoles per coverslip. Significance determination using ANOVA analysis.

Supplemental Table 1:

Oligo list detailing ssDNA sequences used for cloning, genotyping, qPCR, and guide RNAs.

Supplemental Table 2:

Full DNA sequences of our plasmids used for creation of mutant strains.

Supplemental Table 3:

List of antibodies used for immunofluorescence detection.

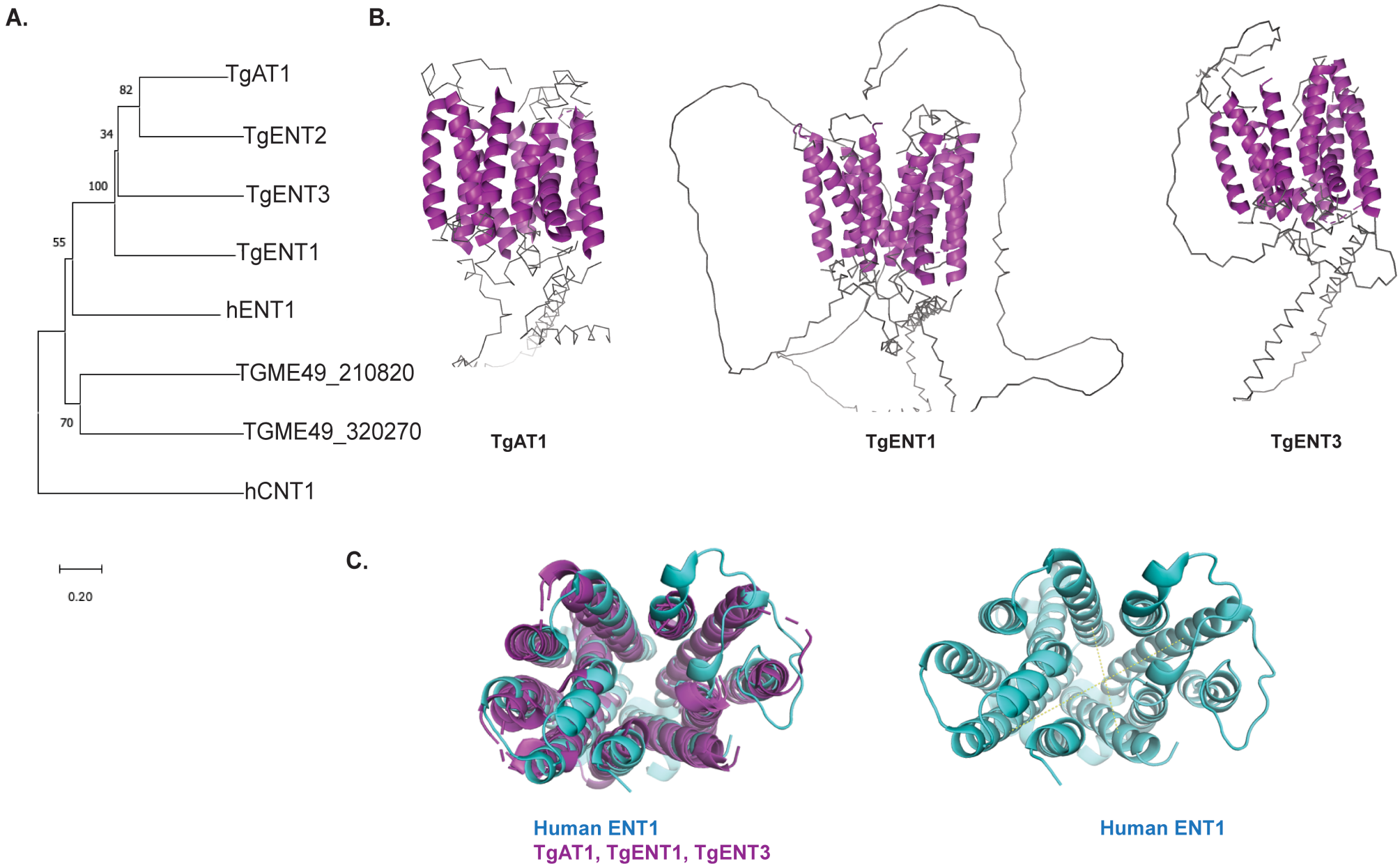
A.
TgAT1
TgENT2
TgENT3
TgENT1
hENT1
TGME49_210820
TGME49_320270
hCNT1
82
34
100
55
70
0.20
B.
TgAT1
TgENT1
TgENT3
C.
Human ENT1
TgAT1, TgENT1, TgENT3
Human ENT1

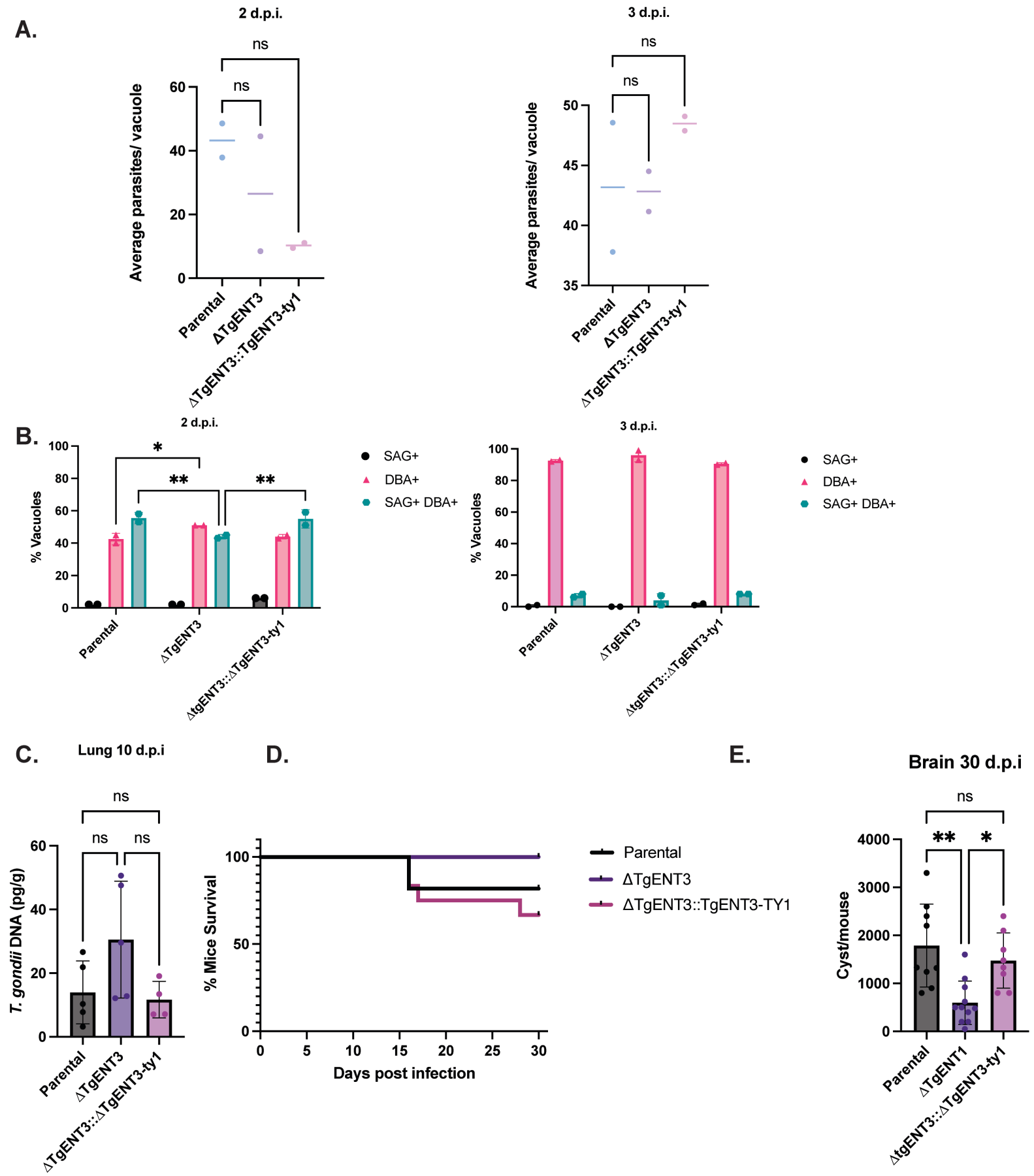
A.
2 d.p.i.
3 d.p.i.
ns
Average parasites/ vacuole
Parental
ΔTgENT3
ΔTgENT3::TgENT3-ty1
B.
% Vacuoles
SAG+
DBA+
SAG+ DBA+
ΔtgENT3::ΔTgENT3-ty1
C.
Lung 10 d.p.i
T. gondii DNA (pg/g)
D.
% Mice Survival
Days post infection
Parental
ΔTgENT3
ΔTgENT3::TgENT3-TY1
E.
Brain 30 d.p.i
Cyst/mouse
ΔTgENT1

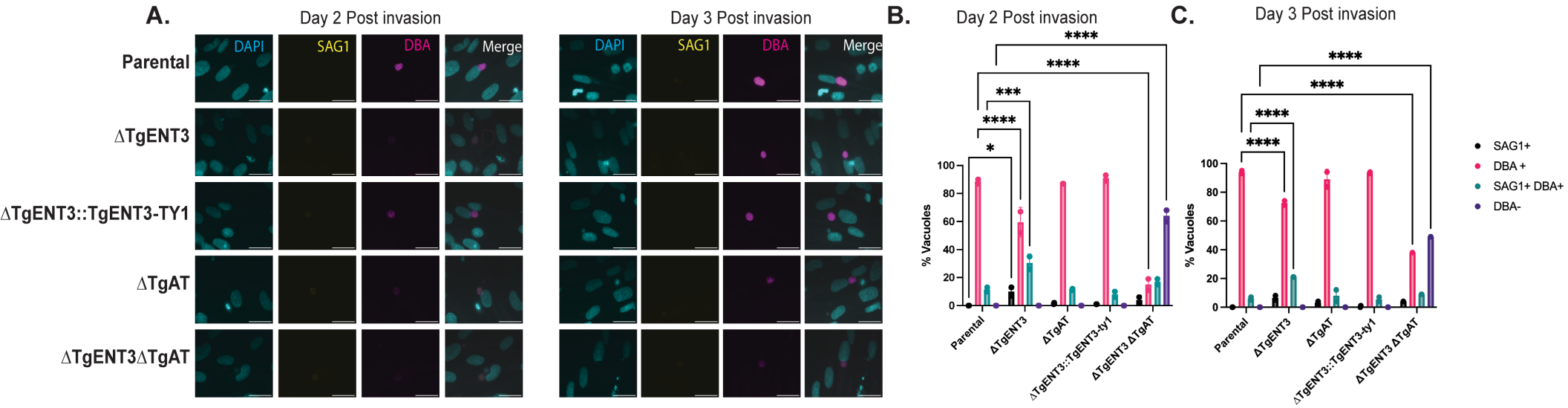
A.
Day 2 Post invasion
Day 3 Post invasion
DAPI
SAG1
DBA
Merge
Parental
ΔTgENT3
ΔTgENT3::TgENT3-TY1
ΔTgAT
ΔTgENT3ΔTgAT
B.
Day 2 Post invasion
C.
Day 3 Post invasion
% Vacuoles
0
20
40
60
80
100
*
***
****
Parental
ΔTgENT3
ΔTgAT
ΔTgENT3::TgENT3-ty1
ΔTgENT3 ΔTgAT
SAG1+
DBA +
SAG1+ DBA+
DBA-

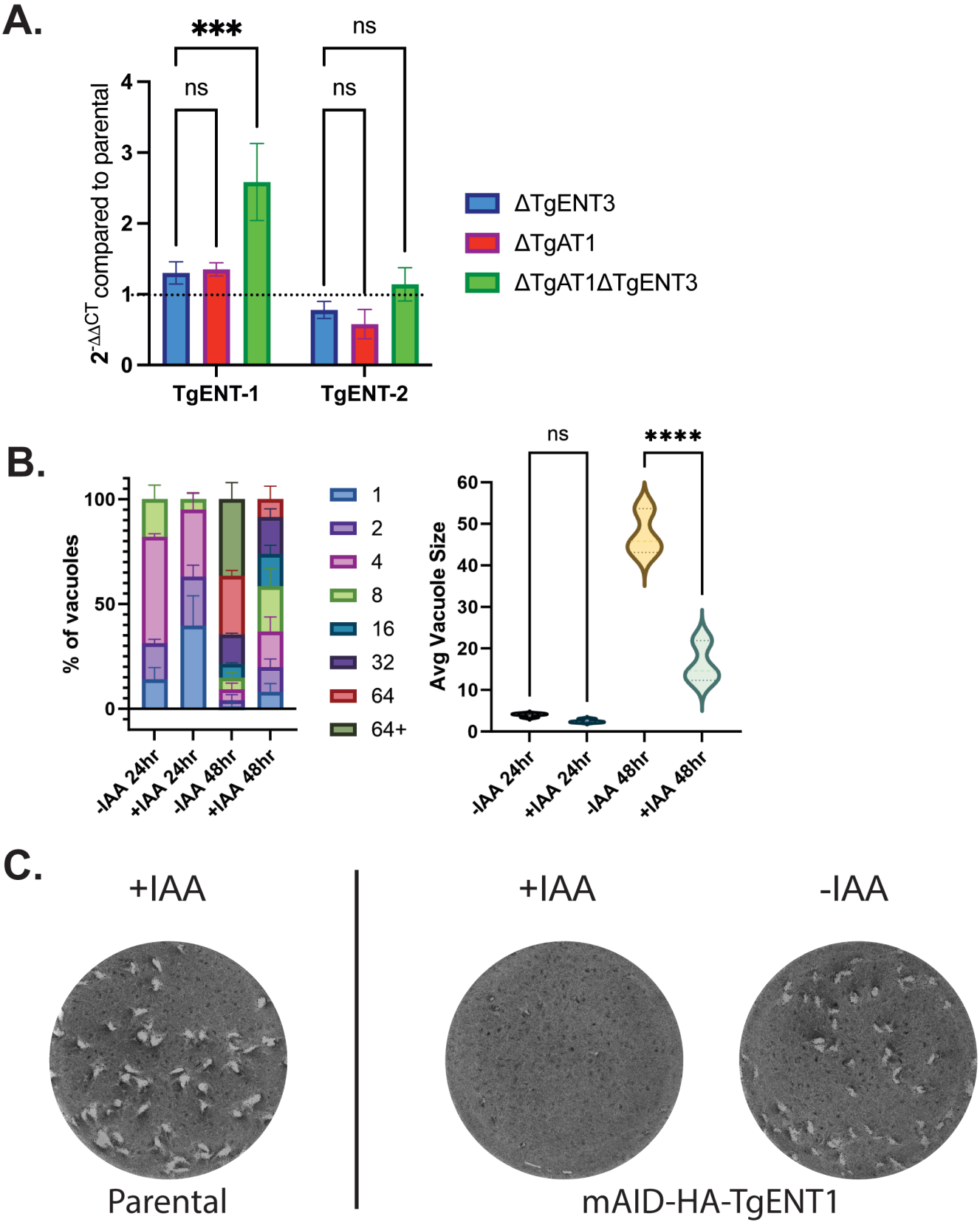
A.
***
ns
ns
ns
$2^{-\Delta\Delta CT}$ compared to parental
0
1
2
3
4
TgENT-1
TgENT-2
ΔTgENT3
ΔTgAT1
ΔTgAT1ΔTgENT3
B.
% of vacuoles
0
50
100
-IAA 24hr
+IAA 24hr
-IAA 48hr
+IAA 48hr
1
2
4
8
16
32
64
64+
ns
****
Avg Vacuole Size
0
10
20
30
40
50
60
-IAA 24hr
+IAA 24hr
-IAA 48hr
+IAA 48hr
C.
+IAA
Parental
+IAA
-IAA
mAID-HA-TgENT1

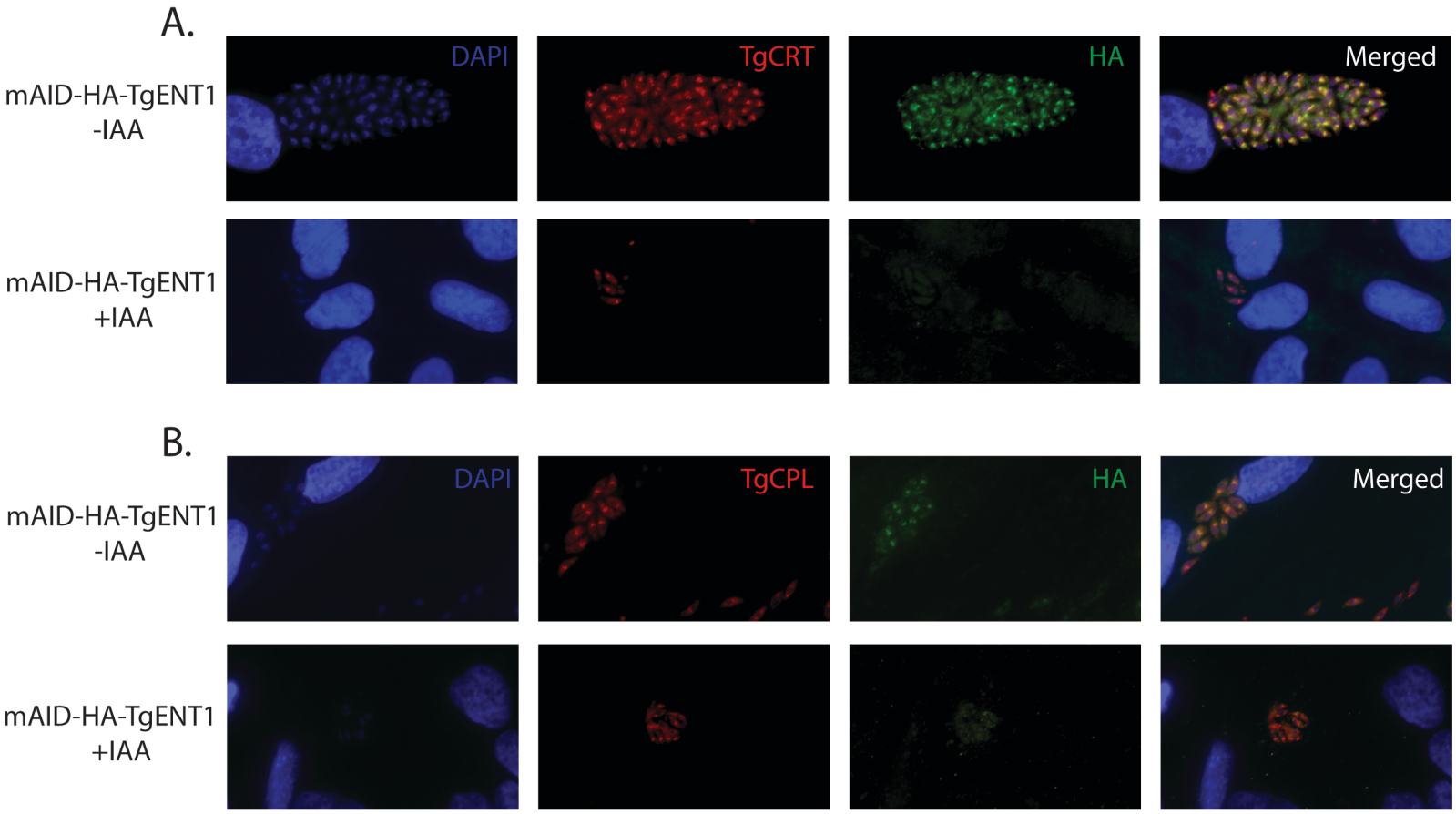
A.
mAID-HA-TgENT1
-IAA
mAID-HA-TgENT1
+IAA
DAPI
TgCRT
HA
Merged
B.
mAID-HA-TgENT1
-IAA
mAID-HA-TgENT1
+IAA
DAPI
TgCPL
HA
Merged